Structure, electron-transport properties, and giant magnetoresistance of hole-doped $LaMnO_3$ systems

R. Mahendiran, S. K. Tiwary, A. K. Raychaudhuri,* and T. V. Ramakrishnan*
Department of Physics, Indian Institute of Science, Bangalore 560012, India

R. Mahesh, N. Rangavittal, and C. N. R. Rao*
Solid State and Structural Chemistry Unit, Indian Institute of Science, Bangalore 560012, India
(Received 12 May 1995; revised manuscript received 5 September 1995)

Results of a detailed investigation of the structure and electron-transport properties of $La_{1-x}A_xMnO_3$ (A =Ca, Sr) over a wide range of compositions are presented along with those of parent $LaMnO_3$ containing different percentages of Mn^{4+}. The electrical resistivity (ρ) and magnetoresistance (MR) of polycrystalline pellets have been measured in the 4.2–400 K range in magnetic fields up to 6 T and the Seebeck coefficient (S) from 100 to 400 K. The electrical measurements were supplemented by ac susceptibility and magnetization measurements. MR is large and negative over a substantial range of compositions and peaks around temperatures close to the ferromagnetic transition temperatures (T_c). An insulator to metal-like transition occurs near the T_c and the temperature dependence of ρ below T_c is related to the magnetization although ρ in the metallic state is generally much larger than the Mott's maximum metallic resistivity. The occurrence of giant magnetoresistance is linked to the presence of an optimal proportion of Mn^{4+} ions and is found in the rhombohedral and the cubic structures where the Mn-O distance is less than 1.97 Å and the Mn-O-Mn angle is $170°\pm10°$. The field dependence of MR shows the presence of two distinct regimes. The thermopower S shows a positive peak in the composition range at a temperature where MR also peaks; S becomes more negative with increase in Mn^{4+}.

I. INTRODUCTION

Giant negative magnetoresistance (GMR) was first observed in Fe/Cr films with antiferromagnetically coupled multilayers.[1] The mechanism of GMR in this system was attributed to the interfacial spin-dependent scattering of conduction electrons.[2] GMR has also been seen in granular heterogeneous Cu-Co and Ag-Co magnetic alloy films.[3] Magnetic semiconductors such as n-type EuO, EuS, EuSe, and Gd-doped EuSe (with carrier concentration $n\approx4\times10^{18}$–3×10^{19} cm^{-3}) as well as $Cd_{0.95}Mn_{0.05}Se$ doped with In or Ga ($n\approx3\times10^{17}$ cm^{-3}) exhibit this phenomenon at low temperatures due to the formation of magnetic polarons.[4–7] The magnitude of MR in these systems is highest when the carrier concentration is close to the critical concentration (n_c) corresponding to the insulator-to-metal transition. The recent observation of GMR in films and single crystals as well as polycrystalline pellets of hole-doped $LaMnO_3$ of the general composition $La_{1-x}A_xMnO_3$ is noteworthy.[8–15] In this oxide system, the transition from the insulating to the metal-like state is brought about by changing the temperature and the magnetoresistance shows a maximum in the temperature range of this transition. In these manganates, the presence of a sufficient proportion of Mn^{4+} ions gives rise to ferromagnetism by the Zener double-exchange mechanism.[16] The temperature T_m at which MR is maximum is generally close to the ferromagnetic transition temperature T_c. In the range of doping where one observes GMR, the zero-field resistivity shows a peak at a temperature T_p, which is also close to T_c. Below T_p, the resistance decreases as the temperature decreases ($d\rho/dT>0$) indicating a metal-like electron transport. Typically, T_m lies in the range $100<T_m<320$ K and generally increases with the radius of the A ion.

In order to understand the phenomenon of GMR in these oxides and the various factors affecting it, we have carried out a systematic investigation of the electron transport and magnetic properties of well-characterized polycrystalline samples of $La_{1-x}A_xMnO_3$ (A=Ca,Sr) over a wide range of compositions. In addition, we have studied the parent $LaMnO_3$ system by varying the Mn^{4+} content by chemical or electrochemical means.[17] It should be noted that Mn^{4+} in $LaMnO_3$ is created by the presence of random cation vacancies in the La and Mn sites, since excess oxygen cannot be accommodated in a perovskite structure.[18] We therefore describe the parent manganate by the formula $La_{1-\delta}Mn_{1-\delta}O_3$ where δ determines the Mn^{4+} content. Besides carrying out magnetic and electron-transport measurements, we have determined the structures of the manganates in order to correlate the magnitude of the MR as well as the other relevant properties of these oxides with the structural parameters. The present investigation has enabled us to understand the role of the structure and the Mn^{4+} content in determining the GMR as well as other factors affecting electron transport in these systems. Among the various aspects examined, mention must be made of the field dependence of the MR at different temperatures and for different Mn^{4+} contents, the magnitude of the resistivity associated with the unusual ''metallic'' state at $T<T_c$, and the temperature variation of the thermopower.

II. EXPERIMENT

$LaMnO_3$ prepared by solid-state reaction of La_2O_3 and MnO_2 was orthorhombic and had 12% Mn^{4+}. Orthorhombic

TABLE I. Structural data and Mn^{4+} content in $La_{1-x}A_xMnO_3$ and $La_{1-\delta}Mn_{1-\delta}O_3$ samples.

Composition	x or δ	Mn^{4+} (%)	Crystal structure[a]	Lattice parameters (Å) or (°)	r_{MO} (Å)	Mn-O-Mn (ϕ°)
$La_{1-x}Ca_xMnO_3$	0.1	19	*R*	$a=5.480$	1.954	164
				$\alpha=60.40$		
	0.2	25	*C*	$a=7.744$	1.944	180
	0.3	33	*C*	$a=7.699$	1.936	180
	0.4	39	*C*	$a=7.677$	1.931	180
	0.5	44	*C*	$a=7.668$	1.922	180
$La_{1-x}Sr_xMnO_3$	0.1	27	*R*	$a=5.523$	1.964	164
				$\alpha=60.60$		
	0.2	34	*R*	$a=5.482$	1.959	164
				$\alpha=60.40$		
	0.3	37	*R*	$a=5.454$	1.953	164
				$\alpha=60.14$		
	0.4	41	*C*	$a=7.721$	1.939	180
	0.5	47	*C*	$a=7.714$	1.932	180
$La_{1-\delta}Mn_{1-\delta}O_3$	0.02	12	*O*	$a=5.543$		
				$b=5.594$	2.034	152
				$c=7.805$		
	0.04	24	*R*	$a=5.478$	1.957	167
				$\alpha=60.55$		
	0.045	33	*C*	$a=7.788$	1.948	180

[a]*O* is orthorhombic, *R* rhombohedral, and *C* cubic.

$LaMnO_3$ was oxidized by heating in an oxygen atmosphere or electrochemically to obtain compositions with 24% and 33% Mn^{4+}. The unit-cell parameters of these samples are shown in Table I. The oxides of the general formula $La_{1-x}A_xMnO_3$ (A=Ca or Sr) were prepared by heating stoichiometric mixtures of La_2O_3, $CaCO_3$, $SrCO_3$, and MnO_2 at 1223 K for 12 h. The reacted powder, obtained after heating, was ground, pelletized, and reheated to 1223 K for another 12 h. The phase purity was checked by x-ray diffraction (using radiation). In Table I we list the unit-cell parameters of the different compositions. An essential aspect of characterization of the manganates is the Mn^{4+} content. The Mn^{4+} content of the samples was determined by redox titrations using potassium permanganate and ferrous sulfate. In Table I we list the Mn^{4+} content of the various samples studied by us.

The structures of $LaMnO_3$ and $La_{1-x}A_xMnO_3$ were investigated by Rietveld treatment of the x-ray diffraction (XRD) profiles recorded with a high-resolution STOE diffractometer. The diffraction profiles were fitted with a Pearson-VII-type function. Data were corrected for absorption effects. The parameters refined were cell dimensions, 2θ zero point, half-width, and background parameters. Subsequently structural parameters were refined to a low R factor.

The ferromagnetic transition temperatures (T_c) obtained from ac susceptibility and magnetization measurements are listed in Table II along with other relevant information. The ac magnetic field for the χ measurements was 1 mT so that the measured χ was in the range of reversible magnetization. We have measured magnetization (M) down to 4.2 K in a field up to 5.5 T for some of the compositions. The T_c values obtained from χ and M measurements as well as the Curie temperature obtained from χ data at $T>T_c$ all agree to within 5 K for the materials with Mn^{4+} content of 20–40 %. The electrical resistivity $\rho(T)$ was measured in the temperature range 4.2–400 K using the four-probe dc or ac (20 Hz) technique. The thermopower was measured by a dc technique by applying heat at one end of a pellet and measuring the resulting thermo emf from a couple of the sample and a Cu wire. The differential temperature was measured by a Au(Fe):Chromel thermocouple.

III. RESULTS

A. Structural aspects

In parent $LaMnO_3$, the composition with 12% Mn^{4+} is orthorhombic while the compositions with 24% and 33% Mn^{4+} are rhombohedral and cubic, respectively. High percentages of Mn^{4+} in these materials are created by the random presence of cation vacancies in both La and Mn sites.[18] Accordingly, the compositions of $LaMnO_3$ written as $La_{1-\delta}Mn_{1-\delta}O_3$ give $\delta=0.02$ for the sample with 12% Mn^{4+}. For the samples with 24% and 33% Mn^{4+}, $\delta=0.04$ and 0.055, respectively. Such cation-deficient samples are erroneously described as $LaMnO_{3+\delta}$ in the literature (see Ref. 18 for details). In $La_{1-x}A_xMnO_3$ (A=Ca,Sr), the orthorhombic structure of the $x=0.0$ composition changes to rhombohedral and then to cubic with increase in Mn^{4+} content (see Table I). In $La_{1-x}Sr_xMnO_3$, the structure is rhombohedral when x is in the 0.1–0.3 range and cubic when $x=0.4$ and 0.5. In the Ca-substituted samples, only the $x=0.1$ composition is rhombohedral and the compositions with $x=0.2$–0.5 are cubic.

TABLE II. Electron-transport and magnetic properties of $La_{1-x}A_xMnO_3$ (A=Ca,Sr) and $La_{1-\delta}Mn_{1-\delta}O_3$. T_c is the ferromagnetic Curie temperature as determined from ac χ and magnetization measurements. T_p is the temperature corresponding to the resistivity peak for $H=0$ T. T_m is the temperature corresponding to the MR peak for H=6 T. $|\delta\rho/\rho(0)|_m$ is the peak value of MR at $T=T_m$. E_a is the activation energy calculated from resistivity data.

Composition	x or δ	Mn^{4+} (%)	T_c (K)	T_p (K)	T_m (K)	$\lvert\delta\rho/\rho(0)\rvert_m$ (%)	E_a (eV)
$La_{1-x}Ca_xMnO_3$	0.1	19	245	225	240	72	0.16
	0.2	25	260	242	242	52	0.16
	0.3	33	260	260	260	55	0.13
	0.4	39	240	235	[a]	42	
	0.5	44	240	100	100	90	0.11
	0.9	86	100[b]	[c]	25	70	0.03
$La_{1-x}Sr_xMnO_3$	0.1	27	260	260	260	44	[e]
	0.2	34	320	270	[d]	46	[e]
	0.3	37	360	330	[d]	45	[e]
	0.4	41	315	290	[d]	44	[e]
	0.5	47	300	[c]	[d]	34	[e]
$La_{1-\delta}Mn_{1-\delta}O_3$	0.02	12	240	[c]	[d]	12	0.24
	0.04	24	230	180	185	53	0.17
	0.055	33	240	200	190	68	0.13

[a]No peak but a broad maximum.
[b]The observed transition at this temperature is tentatively identified as T_c.
[c]No peak in resistivity down to 4.2 K.
[d]No peak in MR down to 4.2 K.
[e]Data at high temperature are insufficient to determine E_a.

Only the rhombohedral and cubic samples with a relatively high Mn^{4+} content show ferromagnetism as well as the associated resistivity maxima (insulator-metal transition) at a temperature T_p close to the Curie temperature T_c. GMR is also found only in these compositions as discussed later.

A careful investigation of the structures of $La_{1-x}A_xMnO_3$ (A=Sr,Ca) as well as $La_{1-\delta}Mn_{1-\delta}O_3$ compounds by Rietveld treatment of the XRD profiles has provided the Mn-O-Mn angles (ϕ) and the Mn-O bond lengths r_{MO}. These are listed in Table I. In Fig. 1, we have plotted both r_{MO} and ϕ against the Mn^{4+} content in the samples. It is interesting that, in all the samples which exhibit the resistivity maxima, ferromagnetism, and GMR, r_{MO} is less than 1.97 Å. In the cubic compositions which generally show the highest T_c (see Table II), $r_{MO}\approx 1.92-1.95$ Å; we would expect r_{MO} to decrease because of the higher Mn^{4+} content. This will lead to a greater overlap of orbitals between the metal and oxygen, a larger transfer integral. This in turn will lead to increased T_c. The Mn-O-Mn angle (ϕ) is 152° in orthorhombic $La_{0.98}Mn_{0.98}O_3$ which is an insulator. However, it is around 162°–167° in the rhombohedral compositions and 180° in the cubic samples. It is to be noted that 180° cation-anion-cation interaction favors ferromagnetism and itinerant d-electron behavior.

B. $La_{1-x}A_xMnO_3$ (A=Ca or Sr) systems

In Fig. 2(a) we show the temperature dependence of the ac susceptibility χ. We have plotted χ as a change normalized with respect to the value at 300 K in the figure. In Fig. 2(b), we show the magnetization M (measured at $H=1.5$ T) as a function of T for the samples $x=0.2$ and 0.9. The first sample has optimal Mn^{4+} content for ferromagnetism while the other has excess Mn^{4+}. The $x=0.9$ sample is supposed to be an antiferromagnet,[19,20] but it does show a ferromagnetic transition at $T<100$ K. The sample has, however, a low value of magnetization. It may be that in this composition range due to chemical inhomogeneities there are small ferromagnetic clusters embedded in an antiferromagnetic or paramagnetic matrix. On increasing x from a low value, the T_c as well as the saturation magnetization first increase, reach a plateau for $x\approx 0.2-0.4$, and then decrease again. For $x>0.4$, one observes broadening of the ferromagnetic transition.

The $\rho(T)$ data of the $La_{1-x}Ca_xMnO_3$ samples with $0.1\leqslant x\leqslant 0.9$ are shown in Fig. 3. In all the samples (except $x=0.9$), ρ first increases as T decreases, exhibits a peak at $T=T_p$ ($\approx T_c$), and then decreases as T is further reduced below T_c. For $T>T_c$, the resistivity shows activated transport as in an insulator, following,

$$\rho(T)=\rho_0\ \exp(E_a/k_BT), \tag{1}$$

where E_a is the activation energy. The peak temperatures (T_p) for the different samples are shown in Table II. For low x, T_p increases as x increases, reaches a maximum when $x=0.3$, and decreases with a further increase of x.

There are several observations which are noteworthy.

(1) In all the samples, except when $x=0.9$, the resistivity at the highest temperature measured ($\rho_{400\ \mathrm{K}}$) is less than that at 4.2 K ($\rho_{4.2\ \mathrm{K}}$) although for $T<T_p$ the material shows a metal-like variation of ρ with temperature ($d\rho/dT>0$). For $T<4.2$ K, the resistivity tends to a residual resistance like

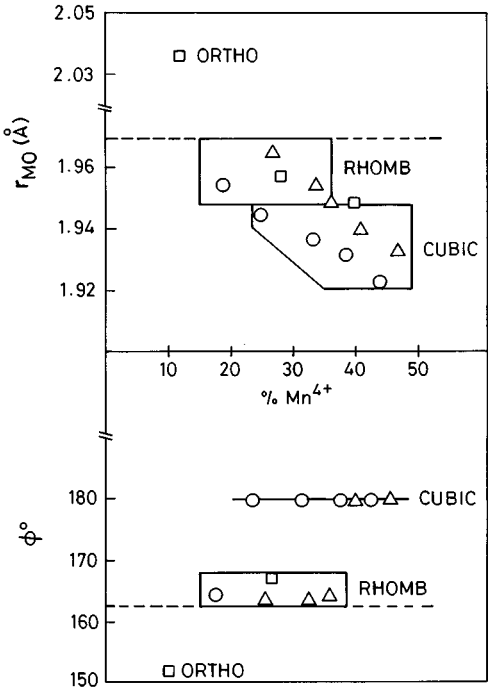

FIG. 1. Variation of Mn-O distance (r_{MO}) and Mn-O-Mn angle (ϕ) with the % Mn^{4+} content in $La_{1-x}A_xMnO_3$: circles, Ca; triangles, Sr; squares, $La_{1-\delta}Mn_{1-\delta}O_3$ compositions.

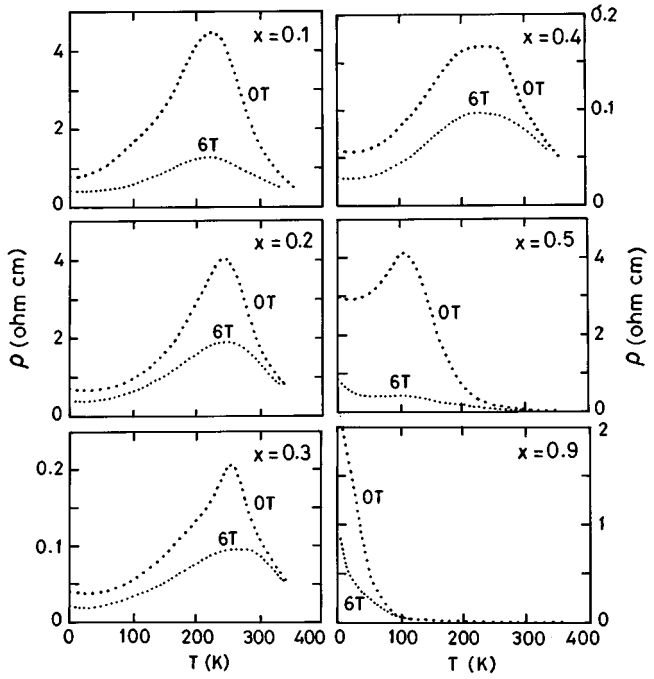

FIG. 3. Temperature variation of resistivities of polycrystalline pellets of $La_{1-x}Ca_xMnO_3$ at $H=0$ and 6 T.

that of a conventional metal or shows a small rise as T decreases. In either case, the limiting low-temperature resistivity ρ_0 (at $T=0$) in the ferromagnetic metal-like phase is higher than the resistivity in the paramagnetic phase (at $T \gg T_c$).

(2) The value of $\rho_{400\ K}$ decreases continuously as x increases and is lowest in the sample with $x=0.9$. The E_a value in the paramagnetic regime decreases progressively as x increases (see Table II).

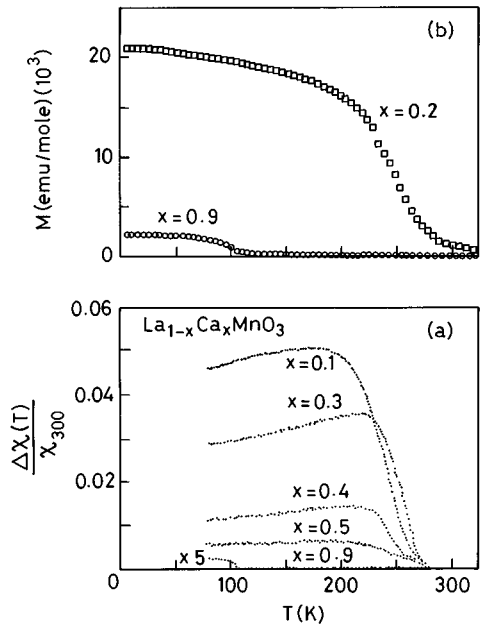

FIG. 2. (a) Relative change in ac susceptibility, $\Delta\chi(T)/\chi(300)$, with temperature for $La_{1-x}Ca_xMnO_3$. (b) Magnetization data for the $x=0.2$ and 0.9 compositions ($H=1.5$ T).

(3) Although one observes metal-like behavior when $T<T_p$, the value of resistivity is very high. The lowest $\rho_{4.2\ K}$ is ~ 30 mΩ cm which is larger than the typical resistivity ρ_{Mott}, which we define as $\rho_{Mott}=1/\sigma_{Mott}$, σ_{Mott} being the Mott minimum metallic conductivity.[21] The estimated ρ_{Mott} for this type of material ≈ 5–10 mΩ cm.[22] Part of the high resistivity may be due to grain boundaries.

In Fig. 3, we have shown the resistivity $\rho(H,T)$ in an applied magnetic field of 6 T. The suppression of ρ in the magnetic field persists over the whole temperature range although the effect decreases above T_c. Defining the MR at a given temperature as $\delta\rho/\rho(0)=[\rho(H)-\rho(0)]/\rho(0)$, we find that in all the compositions, except $x=0.9$, MR is negative for $T<T_c$ and becomes smaller as $T \to T_c$. The variation of MR as a function of the applied field at 4.2 K for the $x=0.2$ and 0.9 compositions is shown in Fig. 4(a). Magnetization data as well as magnetoresistance behavior of these compositions are presented in Fig. 4(b). When $x=0.9$, the MR is negative at low temperatures and becomes positive ($\approx$20%) when $T>100$ K. The magnitude of MR generally shows a peak at a temperature T_m. Both T_m and the magnitude of the MR at T_m, $|(\delta\rho/\rho(0))|_m$, depend on the composition x. When $T<T_m$, the MR decreases and reaches a limiting value of around 50–60 % at 4.2 K.

The compositions with $x \leq 0.5$ showing a distinct ferromagnetic transition at T_c show two regimes in the MR vs H curve [Fig. 4(a)]. One is the low-field region (typically for $H \leq 1$ T) where ρ changes rapidly with H. The other is a region for $H>1$ T where ρ changes gradually. In both the regions ρ changes almost linearly with H. The linear dependence of ρ on H in the low-field region is shown in the inset,

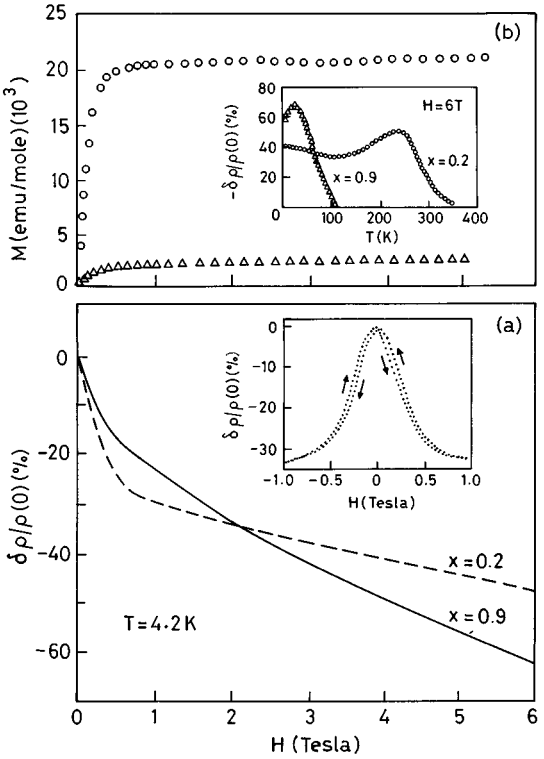

FIG. 4. (a) Variation of magnetoresistance of polycrystalline pellets of $La_{1-x}Ca_xMnO_3$ ($x=0.2,0.9$) with the applied field at $T=4.2$ K. The inset shows MR for $x=0.1$ at $T=4.2$ K for $-1\leq H\leq 1$ T. (b) Magnetization data for the two compositions. Magnetoresistance data are shown in the inset.

where we show the data for the field region $-1<H<1$ T. The two regions in the MR vs H curve are often found in ferromagnetic metals and alloys.[23] This is similar to the dependence of the magnetization (M) on H. The low-field region arises from the motion of domain walls and the high-field region arises from the gradual increase of the spontaneous magnetization on application of the magnetic field. Although this type of variation of MR with H is expected for a ferromagnetic material, there is an important difference. In a strong ferromagnet, the MR shows some anisotropy, but there is no anisotropy in the manganates.

The variation of MR with H is somewhat different in the Ca-rich $La_{0.1}Ca_{0.9}MnO_3$ (see the inset of Fig. 4) which is likely to be an antiferromagnet at $T=4.2$ K. In this material, the distinction between the two regions is not clear although there is a small linear region for $H\leq 0.2$ T. For $H>0.2$ T, the field dependence is not linear. The magnitude of the MR increases with H but the gradient continuously decreases with increase in H, as found in some of the metallic alloys.[24] In the $H>1$ T regime, ρ changes gradually and one also sees a distinct knee in the M-H curve. It is interesting that the $x=0.9$ composition shows large MR, but does not show a metal-insulator transition.

The $\chi(T)$ behavior of the $La_{1-x}Sr_xMnO_3$ system near T_c is similar to that of $La_{1-x}Ca_xMnO_3$. We list the values of T_c in Table II along with the electron-transport parameters for this system. In the Sr-doped system, the values of ρ are lower than in the Ca system, the lowest resistance being found in the $x=0.3$ composition ($\rho_{4.2\ \mathrm{K}}\approx 8$ mΩ cm). The variation of

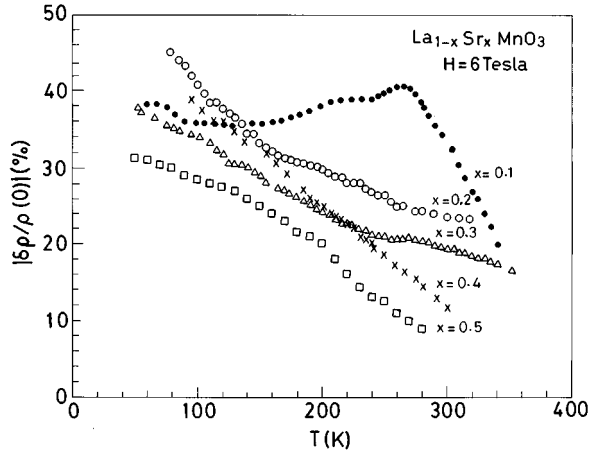

FIG. 5. Temperature variation of magnetoresistance of polycrystalline pellets of $La_{1-x}Sr_xMnO_3$ ($H=6$ T).

MR with temperature (for a fixed field of 6 T) in the Sr system (Fig. 5) is also different from that of the Ca-doped system (Fig. 4). First, the MR for a given field and composition (% Mn^{4+}) is somewhat smaller in the Sr-doped system. Second, while the MR shows a peak at a certain temperature T_m for all values of x in the Ca-doped system, the Sr-doped system shows the peak only in the $x=0.1$ composition with the highest ρ. For the other compositions,[11] the magnitude of the MR monotonically decreases with T or shows a plateau in the region of T_c. In the films of the Sr-doped compositions,[11] however, the MR shows a peak around T_c.

We use the data on the $La_{1-x}Sr_xMnO_3$ system to illustrate the dependence of the MR on H at different T. This is shown in Fig. 6 for two compositions. Like the Ca-substituted system, the Sr-substituted system also shows two regimes in the variation of MR with H for $T\ll T_c$. However, the distinction between the two regions vanishes as $T\rightarrow T_c$, indicating that the contribution of the ferromagnetic domains to the MR is very small close to T_c. It is to be noted that the peak in the MR occurs in this region ($T_m\approx T_c$). For instance, for the $La_{0.9}Sr_{0.1}MnO_3$ sample, the peak in the MR occurs at 260 K and at this temperature the two regimes in the MR vs H curve are not seen and one observes only a smooth variation. For the Sr-substituted sample with $x=0.5$ one does not see any insulator-metal transition and it has a broad ferromagnetic transition. In this material, the two regimes in the MR vs H curve do not manifest themselves till $T<150$ K (i.e., $T/T_c<0.6$).

C. The $LaMnO_3$ system

Our study of the $LaMnO_3$ compositions (without any divalent cation doping) is significant since it helps to demonstrate the seminal role of Mn^{4+} ions in the structure as well as in the electron transport in these materials. We notice that cubic $La_{0.945}Mn_{0.945}O_3$ (Mn^{4+} 33%) and rhombohedral $La_{0.96}Mn_{0.96}O_3$ (Mn^{4+} 24%) show sharp ferromagnetic transitions. In Fig. 7, we present the ρ vs T data on the cubic $La_{0.945}Mn_{0.945}O_3$ sample at zero field and for six field values from 1 to 7 T. Magnetization and susceptibility data for this cubic oxide are also given in this figure. We find that the T_c

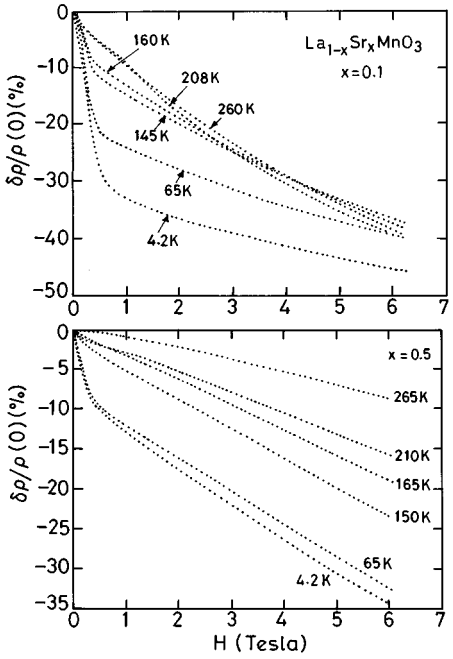

FIG. 6. Variation of magnetoresistance with magnetic field for two compositions of $La_{1-x}Sr_xMnO_3$ ($x=0.1,0.5$) at different temperatures.

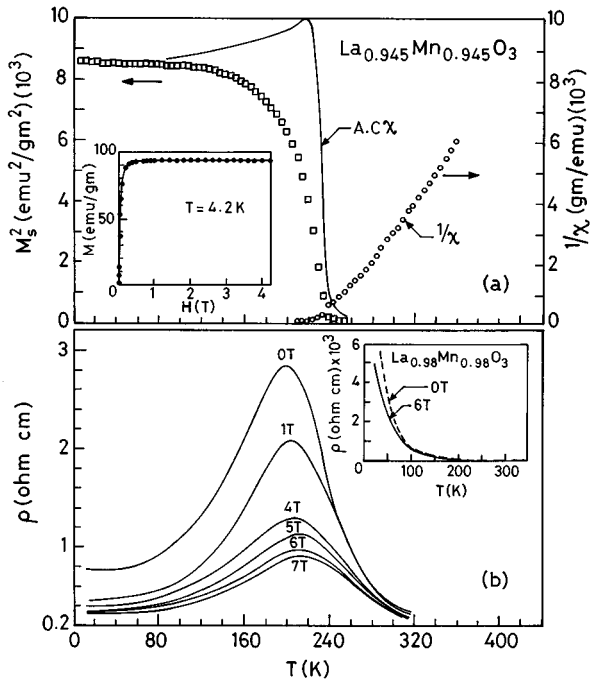

FIG. 7. (a) Magnetization and ac susceptibility data for $La_{0.945}Mn_{0.945}O_3$. (The ac χ has an arbitrary scale.) Inset shows magnetization at 4.2 K as a function of field strength. (b) Temperature variation of resistivity of a polycrystalline pellet of cubic $La_{0.945}Mn_{0.945}O_3$ for different values of H. Inset shows the resistivity data for $La_{0.98}Mn_{0.98}O_3$ (orthorhombic) at 0 and 6 T.

values of the $LaMnO_3$ samples from the various magnetic measurements are within a few Kelvin. The saturation magnetization of the cubic sample is $3.8\mu_B$, indicating that this is as good a ferromagnet as the corresponding Ca-substituted manganate. In the inset of Fig. 7(b), we show the ρ-T data for the orthorhombic sample of the composition $La_{0.98}Mn_{0.98}O_3$. The various parameters for the $LaMnO_3$ system are listed in Table II. The orthorhombic sample ($\delta=0.02$) is insulating at all temperatures. The resistivities of the rhombohedral and cubic samples with $\delta=0.04$ and 0.055 show distinct T_p and metal-like behavior when $T<T_p$. The resistivity of these samples is very high and ρ_p is around 3 Ω cm even in the cubic sample, a value larger than in the Ca- or the Sr-doped system with the same Mn^{4+} concentration.

The temperature dependence of the MR of the cubic and the rhombohedral samples is similar to that of the Ca-doped samples with a peak at T_m (180–220 K). The dependence of MR on H is also similar to that of the Ca-doped samples. The MR in the orthorhombic sample, which stays insulating over the whole temperature range, is very small ($\leqslant$10%) and the MR does not show any peak. The data presented in Fig. 7 on the cubic $La_{0.945}Mn_{0.945}O_3$ sample at different fields are typical of all the hole-doped $LaMnO_3$ systems which exhibit large MR. The figure clearly shows that though the MR is present at all temperatures the field dependence of MR depends on the temperature of the measurement. At low temperature ($T\ll T_c$) most of the changes occur at low fields ($H<2$ T) with a slow increase in MR for $H>2$ T. In the region close to T_m (which in turn is close to T_c) the change in MR is more uniform over the whole field region. As pointed out earlier, this type of dependence of MR on the applied field arises when the spontaneous magnetization gradually increases with the applied field.

D. Thermopower measurements

In Fig. 8 we have shown the thermopower (S) of the $La_{1-x}Ca_xMnO_3$ samples over the temperature range 100–350 K which encompasses the region of T_c. At high temperatures, S approaches a constant value which is negative for the samples with $x\geqslant 0.2$; S becomes more negative as x (or the Mn^{4+} content) increases. The dependence of S on x is shown in the inset of Fig. 8 at two temperatures. There is a distinct positive shift of S when the temperature is closer to T_c. For the $x=0.1$ sample, the high-temperature limiting value of S is small and may be either positive or negative. For the $x=0.9$ sample, the thermopower is negative and large and is essentially temperature independent down to 100 K. As the temperature is decreased, there is a positive contribution peaking around T_m. The positive contribution is more significant in the $x=0.1$ and 0.2 samples, for which the total observed thermopower actually peaks at T_m. At $T\ll T_c$, the thermopower is small ($|S|\leqslant 10$ μV/K). The positive thermopower near T_m is clearly seen in the cation-deficient $La_{1-\delta}Mn_{1-\delta}O_3$ samples which show large MR. We see this in Fig. 9 where the thermopowers of the cubic ($\delta=0.055$) and the rhombohedral ($\delta=0.04$) samples are shown. In this figure, we also show the data for the $La_{0.9}Ca_{0.1}MnO_3$ sample. The peaks in S near T_m are nearly identical in the three samples.

IV. DISCUSSION

A. Correlations of MR and related experimental quantities with structure and composition

Our investigations of the structure, electron transport, and magnetoresistance of the $La_{1-x}A_xMnO_3$ (A=Ca and Sr) and

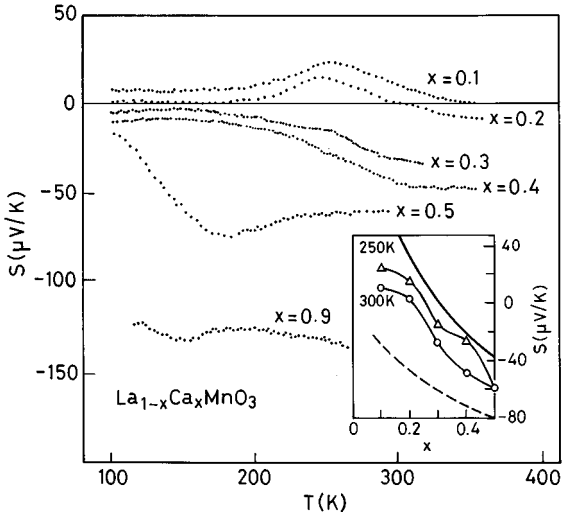

FIG. 8. Thermopower of the $La_{1-x}Ca_xMnO_3$ system. The inset shows S at two temperatures. The solid line in the inset refers to the estimate of S based on Eq. (3) with complete correlation and the dashed line is based on Eq. (4) with no correlation.

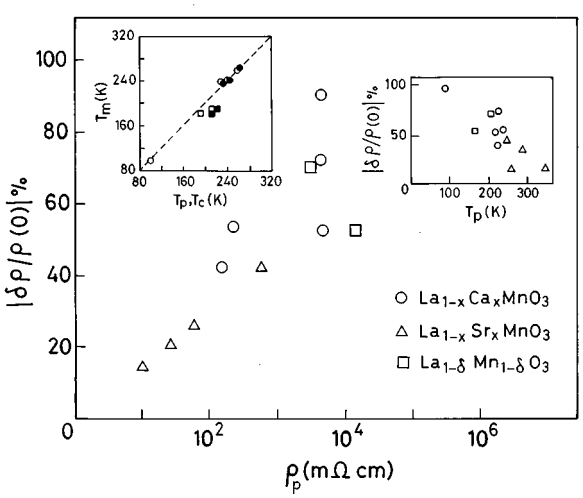

FIG. 10. Variation of the maximum magnetoresistance $\delta\rho/\rho(0)$ at $H=6$ T with the peak value of the resistivity. In the inset on the top left-hand side, T_m is plotted against the ferromagnetic T_c as well as the temperature (T_p) corresponding to the resistivity maximum (closed circles and squares, T_c's of Ca doped and $La_{1-\delta}Mn_{1-\delta}O_3$, respectively; open circles and squares, T_p's of the above systems in the same order). In the other inset, the variation of magnetoresistance with T_p is shown.

$La_{1-\delta}Mn_{1-\delta}O_3$ systems over wide ranges of temperature and composition have enabled us to arrive at certain empirical correlations among the various physical parameters. The value of ρ is an important factor in determining the magnitude of the MR, a high value generally favoring high MR. In Fig. 10 we have plotted the peak magnitude of MR (at $H=6$ T) against ρ_p for all the samples studied. The value of ρ_p spans nearly three decades. The highest ρ_p at which one observes GMR seems to saturate around 10 Ω cm for most of the samples. It was pointed out earlier that MR is generally highest at a temperature T_m which is close to T_c and T_p. Since T_m itself gets shifted to higher values on the application of magnetic field, we designate T_m as the temperature at $H=6$ T. A plot of T_m vs T_c (T_p) shows the experimentally observed points to be roughly around the 45° line although the T_c values tend to be somewhat higher than T_m in some of the samples (see the inset of Fig. 10). In another inset of Fig. 10 we have plotted the peak value of MR against T_p, which shows a decreasing trend in MR with increase in T_p.

The Mn^{4+} content and structural parameters such as the Mn-O distance (r_{MO}) and the metal-oxygen-metal angle (ϕ) play crucial roles in determining MR in the manganates. The mixed valence of Mn (Mn^{3+}/Mn^{4+}) provides the necessary coupling of magnetism and electron transport.[16,25] Rapid hopping of electrons between the ligand and the metal ions (as in Zener double exchange) gives rise to the onset of metal-like behavior in these systems. Such rapid hopping has been seen through Mössbauer studies[26] in a similar mixed-valence oxide system, $La_{1-x}Sr_xCoO_3$.

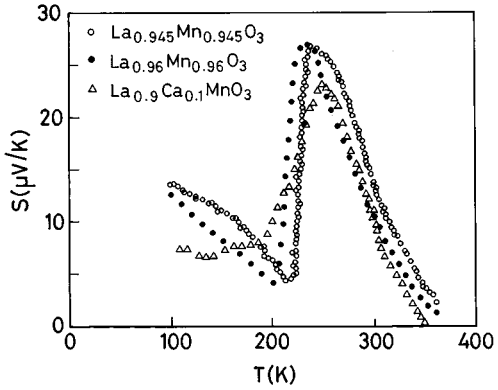

FIG. 9. Thermopower of $La_{1-\delta}Mn_{1-\delta}O_3$ ($\delta=0.04$ and 0.055) and $La_{0.9}Ca_{0.1}MnO_3$.

In Fig. 11 we have plotted $\rho_{4.2\ K}$, T_m, and $(\delta\rho/\rho)_m$ at $H=6$ T against the Mn^{4+} content. In the same figure, we have plotted T_c and the saturation magnetization (M_s). There is a minimum value of Mn^{4+} (≈20%) at which the system becomes metallic and GMR also sets in. Over a certain range of Mn^{4+} content (≈25%–40%), most of the quantities like the GMR, M_s, T_c, and T_m remain constant. The resistivity $\rho_{4.2\ K}$, however, shows a dip at Mn^{4+}≈30%–35%. The Mn^{4+} content of 25%–40% is thus the optimal composition for ferromagnetism as well as GMR. In this region, M_s can be explained as a weighted average of the Mn^{4+} and Mn^{3+} spins. For higher Mn^{4+} content in excess of 50%, the antiferromagnetic interaction of the Mn^{4+}-O-Mn^{4+} and Mn^{3+}-O-Mn^{3+} ion pairs takes over. It is interesting that even in the $La_{0.1}Ca_{0.9}MnO_3$ sample (Mn^{4+}≈86%) there is a ferromagnetic transition at T_c≈100 K. The sample is insulating to the lowest temperature but shows a peak in MR (=70%) at T≈30 K [see the inset of Fig. 4(b)]. This material is not a homogeneous ferromagnet but can have ferromagnetically aligned clusters in a paramagnetic/antiferromagnetic matrix. The clusters themselves may be conducting but their concentration is small enough to make the whole sample ferromagnetic or electrically conducting. Clearly, the concentration as well as the spatial distribution of the Mn^{4+} ions is an important factor determining the electrical and magnetic behavior of the manganates.

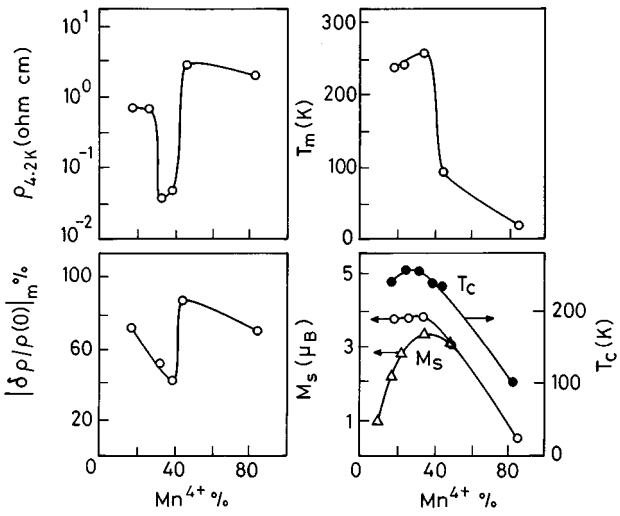

FIG. 11. Dependence of $\rho_{4.2}$, $(\delta\rho/\rho(0))_m$, T_m, M_s (in Bohr magnetons), and T_c of $La_{1-x}Ca_xMnO_3$ on the Mn^{4+} content. M_s data of Ref. 19 are represented by triangles and our data by circles.

The Mn-O distance and the angle ϕ determine the Mn-O overlap integral and hence the electronic properties of the manganates. The dependence on r_{MO} is best seen in the activation energies for transport (E_a) obtained from Eq. (1) and tabulated in Table II. In the paramagnetic regime ($T \gg T_c$), the resistivity decreases continuously as x increases, primarily because of the decrease in E_a. In Fig. 12, we plot E_a and $1/\rho_0$ [$=\sigma_0$, see Eq. (1)] as a function of r_{MO} for two systems. We see that E_a decreases for $r_{MO} < 2$ Å. The factor $1/\rho_0$ is directly proportional to the hopping frequency for charge transfer from the ligand to the cation. Accordingly, we find a rapid rise in $1/\rho_0$ when the r_{MO} is less than 1.94 Å. This is the range where one sees maximum MR. The existence of a critical $r_{MO} \approx 1.97$ Å for the occurrence of GMR implies that there is a minimum strength of the double-exchange interaction required to stabilize the ferromagnetic state and give rise to metal-like electrical conduction. In one of the $LaMnO_3$ systems it has indeed been reported[15] that r_{MO} increases as z decreases and large GMR is seen until

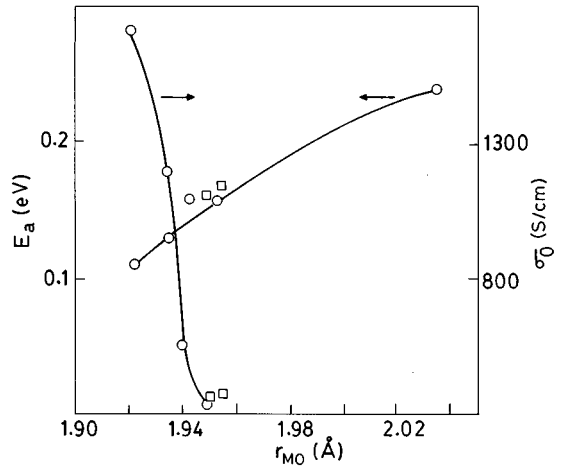

FIG. 12. The dependence of activation energy (E_a) and σ_0 [$=1/\rho_0$ from Eq. (1)] on the bond distance (r_{M0}).

$z \approx 2.80$. When $z = 2.80$, $r_{MO} > 1.96$ Å. An increase in GMR on reducing r_{MO} has been reported[10] in $La_{0.60}Y_{0.07}Ca_{0.33}MnO_3$ where the replacement of La by Y brings about a reduction in r_{MO}. The Mn-O-Mn bond angle ϕ has a role to play in determining E_a and $1/\rho_0$, since the extent of σ bonding arising from the overlap of oxygen (p) and Mn (d) orbitals increases as ϕ approaches 180°. The value of ϕ when Mn^{4+} is ~30% is generally 170°±10°, both the metal-like behavior and GMR being prominent in the cubic phase with $\phi = 180°$.

B. Transport properties

A qualitative picture of the major trends in the properties of the mixed-valent manganates can be given based on the concept of Zener double exchange.[16] The basic ingredient is the hopping of a d hole from Mn^{4+} (d^3, $t_{2g}^{(3)}$, $S = \frac{3}{2}$) to Mn^{3+} (d^4, $t_{2g}^{(3)} e_g^{(1)}$, $S = 2$) via the intervening ligand oxygen, so that Mn^{4+} and Mn^{3+} change places, as in $Mn^{4+}(i)$-O-$Mn^{3+}(j) \rightarrow Mn^{3+}(i)$-O-$Mn^{4+}(j)$, i and j being nearest neighbors. Based on Zener double exchange, we would expect a paramagnetic-to-ferromagnetic transition to occur with a transition temperature

$$k_B T_c \approx x_h \xi t \tag{2}$$

where x_h is the hole concentration, t is the hole hopping amplitude, and ξ is the number of nearest neighbors. Electronically, the system is expected to be a disordered metal in the paramagnetic phase with holes diffusing through a collection of disordered but thermally fluctuating or annealed spins, or a metal in the ferromagnetic phase whose resistivity decreases with temperature as the magnetization grows below T_c. On applying a magnetic field the spins become better aligned, so that holes move more easily and a negative magnetoresistance is expected. Near T_c, the system is magnetically the softest, giving rise to maximum magnetoresistance around this temperature. Some of these expectations are in qualitative agreement with the observations, but there are a few experimental features which have emerged from the present study that need to be understood. They could result from effects of ionic attraction, disorder, the Jahn-Teller effect, or magnetic or lattice polaron formation.

From band-structure calculations,[27] it appears that $t \approx 0.2$ eV so that for $x_h \approx 0.1$ or so a ferromagnetic transition temperature $T_c \approx 2000$ K is expected from Eq. (2). This is about an order of magnitude more than the observed T_c, possibly due to strong Jahn-Teller effects[27] which reduce t. This polaronic effect has a natural phonon temperature scale ($\approx \Theta_D$, the Debye temperature). The observed relative constancy of T_c over a broad range of x (for $0.1 < x < 0.4$) in both $La_{1-x}Sr_xMnO_3$ and $La_{1-x}Ca_xMnO_3$ could be connected with this energy scale. [A picture based on Eq. (2) suggests $T_c \propto x_h \approx x$. Such a dependence of T_c is certainly not observed.]

We have found the resistivity above T_c to have an activated form [Eq. (1)] with an activation energy E_a (in the range 0.25–0.13 eV) decreasing as x increases. The prefactor ρ_0 is of the order of 1 mΩ cm (see Fig. 12), implying that the holes are localized in the paramagnetic phase. This localization is most likely due to either the Coulomb attraction of the divalent ion, or lattice distortion around it. This localization

is aided by the spin disorder in the paramagnetic state. It is an interesting question as to how such a large density of holes can remain localized, and what determines the size of the relatively small activation energy.

Below T_c, there is local ferromagnetic ordering over a length scale which is probably larger than the mean free path of the carriers and long-range magnetic order in a certain composition range. This strongly favors delocalization of holes as the spins become more and more ordered on cooling, enabling holes to move coherently. ρ is of the order of 1 to 0.05 Ω cm for the Ca-doped system. For comparison, the maximum metallic resistivity of Mott (corresponding to a mean free path equal to lattice spacing) is roughly $\rho_{\text{Mott}} \approx 1$–$10$ mΩ cm. Thus we have finite resistivity at $T=0$ even if the ρ is larger than what one would have if the mean free path $\approx$ lattice spacing. This is rather unusual. One generally finds metallic behavior [$\rho(T=0)$ is finite] in oxides for $\rho < 1$–15 Ω cm. For ρ greater than this value, $\rho \rightarrow$ infinity as $T \rightarrow 0$. It is possible that only a small fraction of carriers is free, the others being bound by the local atomic potential. The free holes move in a medium of bound holes and disordered spins. For such a high maximum metallic resistivity, one would expect a carrier density reduction by a factor of $[\rho(T=0)/\rho_{\text{Mott}}]^3 \approx 10^6$. Such a low carrier density is not unlikely given the fact that no measurable density of states has been detected near the Fermi energy by photoemission experiments.[28]

The temperature dependence of ρ below T_c is not well understood. Typically, in a metal, the strength of the electron-phonon interaction is such that $\Delta\rho(300)$ $[=\rho_{(300\ \text{K})}-\rho_{4.2\ \text{K}}] \leqslant 100$ $\mu\Omega$ cm. In metallic oxides $\Delta\rho(300)$ is typically $\leqslant 1$–3 mΩ cm. In the manganates, although $d\rho/dT>0$ in the region $T<T_c$ as in a conventional metal, the temperature dependence of ρ measured as $\Delta\rho(T_c)$ $(=\rho_c-\rho_{4.2\ \text{K}})$ is much larger. For example, in $La_{0.9}Ca_{0.1}MnO_3$ and $La_{0.96}Mn_{0.96}O_3$ samples the observed $\Delta\rho \approx 3$–4 Ω cm. If this large $\Delta\rho$ has to arise from a conventional electron-phonon interaction, the electron-phonon coupling constant has to be unusually large. We can therefore rule out such conventional mechanisms as the cause of the temperature dependence of ρ.

In a ferromagnetic metal, in addition to the electron-phonon interaction, one expects a T^2 term in resistivity arising from the scattering of carriers from the spin waves. The resistivity contribution amongst other things is inversely proportional to D_{SW}^2, where D_{SW} is the spin-wave stiffness constant. We do find evidence of a spin-wave contribution from the temperature dependence of the magnetization M which at low temperatures follows a relation $M=M_0-\alpha T^{3/2}$, where the constant α is related to D_{SW}.[29] From the low-temperature magnetization data of $La_{0.8}Ca_{0.2}MnO_3$ and cubic $La_{0.945}Mn_{0.945}O_3$ we estimate $D_{\text{SW}} \approx 150$–$100$ meV A^2. This is similar to the value in a closely related ferromagnetic metallic oxide $La_{0.6}Sr_{0.4}CoO_3$.[30] In $La_{0.6}Sr_{0.4}CoO_3$, the resistivity is low and one finds a T^2 term with the coefficient $B \approx 10^8$ Ω cm/K^2. If the effective mass of the carriers and the carrier density are similar in the manganates one would expect to see a similar contribution at lower temperatures. It will not, however, be possible to see such a contribution unless the resistivity is low enough ($\leqslant 10$ mΩ cm). Often a small rise in resistivity at low temperatures can mask the T^2 contribution.

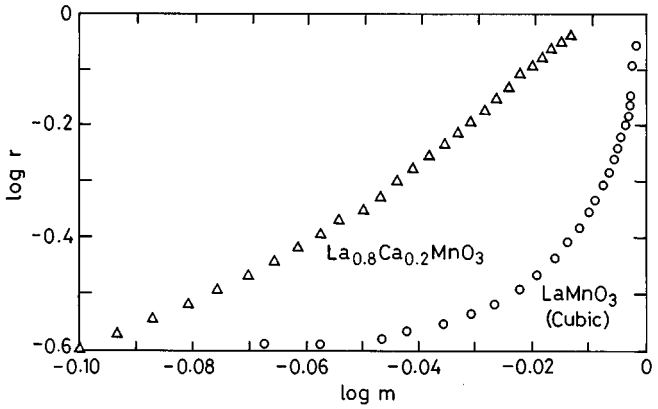

FIG. 13. Plot of r $(=\rho_{4.2}/\rho_T)$ against m $[=M_s(T)/M_s(4.2)]$. Note that both r and m are in log scale.

It therefore seems that the large temperature dependence of ρ cannot be explained by conventional mechanisms.

The metallic state in the manganates is brought about by the onset of ferromagnetic spin order. As the temperature decreases the magnetization M increases and the resistivity decreases. The temperature dependence of ρ below T_c would therefore be expected to reflect the temperature dependence of the spontaneous magnetization M_s. Experimentally, however, it is difficult to find this function exactly because of the influence of other factors on the resistivity. For instance, as $T \rightarrow 0$, $M_s \rightarrow M_s(0)$, a constant, and the resistivity $\rho \rightarrow \rho_0$, a constant. But the constant residual resistivity contains a contribution from extraneous factors such as lattice effects and grain boundaries. Keeping these limitations in mind we have plotted the quantity r $[=\rho_{4.2}/\rho(T)]$ as a function of the scaled magnetization m $[=M_s/M_s(4.2)]$ for two samples, $La_{0.8}Ca_{0.2}MnO_3$ and cubic $LaMnO_3$, in Fig. 13. The quantity r is the scaled conductivity. [$\rho_{4.2}$ and $M_s(4.2)$ are the values of the resistivity and saturation magnetization, respectively, at $T=4.2$ K.] We find that r has a strong dependence on m but it is difficult to find a simple functional form which describes the dependence expected in view of other contributions to the observed ρ.

With regard to the thermopower data, two features are noteworthy: first, the peak in S near T_c in some of the samples with relatively lower Mn^{4+} content, and second, a constant thermopower at high temperatures. A detailed analysis of the thermopower data is beyond the scope of the paper, but we are able to make a few observations on the implications of the data. The peak in S near T_c can arise from the magnetic specific heat (ΔC_m) which near the ferromagnetic transition[31] shows a prominent peak. This peak can be used to get a measure of the entropy involved in the ferromagnetic transition since S measures the entropy of the charge carriers. If we assume that the holes have a strong coupling to the magnetic spins, a part of the entropy of the spins can get added to the entropy of the carriers, much like the phonon drag effect.[23] In that case, we have $S=\frac{1}{3}(\eta \Delta C_m/|e|N)$ where N is the hole concentration and η is a measure of the coupling of the spin entropy to the entropy of the carriers. From the observed data of ΔC_m (≈ 33 J/mol K) and S (≈ 30 μV/K) at $T=T_c$, we find that $\eta \approx 0.05$. The peak in S near T_c seen in some of the compositions thus may be explained by this mechanism. As x is changed, both

N and η will change and the contribution of ΔC_m to S will also change. For instance, as x increases, N will increase and S near the peak will decrease.

In addition to the above terms, there are other contributions to the thermoelectric power. As T increases beyond T_c, S reaches a temperature-independent value. We propose to explain the high-temperature thermopower by Heikes's formula and its suggested modifications.[32] In the limit of high temperature ($T\rightarrow\infty$), the thermopower for a system of localized carriers with spin is given by

$$S(T\rightarrow\infty)\approx-(k_B/|e|)\ln[2(1-c)/c], \tag{3}$$

where c is the relative electron concentration measured as the number of electrons per available site. The above relation assumes complete correlation so that all double occupancy is avoided (on-site Coulomb repulsion $U\gg k_BT$). In the other extreme, when we have no correlation and double occupancy is allowed ($U\ll k_BT$) we have

$$S(T\rightarrow\infty)\approx-(k_B/|e|)\ln[(2-c)/c]. \tag{4}$$

If the hole concentration ($=1-c$) is assumed to be the relative Mn^{4+} concentration, we can estimate the high-temperature limit of S from Eqs. (3) and (4). We have shown these estimates as solid and dashed lines in the inset of Fig. 8. The solid line corresponds to the estimate based on Eq. (3) (complete correlation). It is interesting that the variation of S with x follows the same trend as predicted by the above equations and the observed value of S (at 300 K) is between the two limits of complete and no correlation.

V. CONCLUSIONS

Based on the present investigations, we draw the following conclusions.

(i) The occurrence of GMR is directly linked to the presence of Mn^{4+} in adequate proportion. This is true for both the divalent-metal-substituted manganates and $LaMnO_3$. The highest GMR as well as the optimal values of the associated properties favoring GMR are found around 30% Mn^{4+}.

(ii) GMR is observed in the cubic and rhombohedral phases of the manganates and not in the orthorhombic phase.

(iii) The observed GMR depends on structural parameters such as the Mn-O bond length r_{MO} and the Mn-O-Mn bond angle ϕ. There is a critical value of r_{MO} (1.97 Å) only below which GMR is observed.

(iv) The highest observable GMR seems to increase with the resistivity. The highest ρ for which GMR has been observed in these materials is around 1–10 Ω cm.

(v) Though the MR in a given field peaks around T_c, there is substantial MR even at $T\ll T_c$. Field-dependent MR measurements show two types of regime, the relative importance of which depends on the temperature and the composition.

(vi) Electron transport at $T>T_p$ (T_c) is activated. The metal-like resistivity behavior $\rho(d\rho/dT>0)$ when $T<T_p$ is related to the occurrence of a long-range ferromagnetic state arising from the Mn^{3+}-O-Mn^{4+} interaction. The observed ρ in this metal-like state is much larger than that generally observed in metallic oxides and is far above Mott's metallic resistivity. The temperature dependence of ρ at $T<T_p$ is also unusual.

(vii) The thermopower reaches a limiting negative value at $T\gg T_c$. It has a positive contribution which peaks near T_c. The peak in the thermopower is likely to be related to the magnetic specific heat near the ferromagnetic transition, indicating that there is a strong coupling of the charge carriers with the magnetic spins.

ACKNOWLEDGMENTS

One of us (R.M.) wants to thank the Council of Scientific and Industrial Research for support. A.K.R. thanks the Department of Science and Technology, Government of India, for financial support. We thank H. Ju of the University of Maryland for assistance with magnetization measurements on one of the samples.

*Also at the Jawaharlal Nehru Centre for Advanced Scientific Research, Bangalore 560 064, India.

[1] M. N. Baibich, J. M. Broto, A. Fert, F. Nguyen Van Dan, F. Petroff, P. Etienue, G. Creuzet, A. Friedrich, and J. Chazelas, Phys. Rev. Lett. **61**, 2472 (1988).

[2] P. M. Levy, Solid State Phys. **47**, 367 (1994) and references therein.

[3] A. E. Berkowitz, J. R. Mitchell, M. J. Carey, A. P. Young, D. Rao, A. Starr, S. Zhang, F. E. Spada, F. T. Parker, A. Hutten, and G. Thomas, J. Appl. Phys. **73**, 5320 (1993).

[4] S. von Molnar and S. Methfessel, J. Appl. Phys. **38**, 959 (1967).

[5] Y. Shapira, S. Foner, N. F. Oliveira, Jr., and T. B. Reed, Phys. Rev. B **10**, 4765 (1974).

[6] N. B. Brandt and V. V. Moschalkov, Adv. Phys. **33**, 193 (1984).

[7] T. Dietl, L. Swierkowski, J. Jaroszynski, M. Sawicki, and T. Wojtowicz, Phys. Scr. **T14**, 29 (1986).

[8] K. Chanara, T. Ohno, M. Kasai, and Y. Kozono, Appl. Phys. Lett. **63**, 1990 (1993).

[9] R. Von Helmolt, J. Wecker, B. Holzapfel, L. Schultz, and K. Samwer, Phys. Rev. Lett. **71**, 2331 (1994).

[10] M. McCormack, S. Jin, T. Tiefel, R. M. Fleming, J. M. Phillips, and R. Ramesh, Appl. Phys. Lett. **64**, 3045 (1994); S. Jin, H. M. O. Bryan, T. H. Tiefel, M. McCormack, and W. W. Rhodes, *ibid*. **66**, 382 (1995).

[11] H. L. Ju, C. Kwon, Q. Li, R. L. Greene, and T. Venkatesan, Appl. Phys. Lett. **65**, 2108 (1994).

[12] R. Mahesh, R. Mahendiran, A. K. Raychaudhuri, and C. N. R. Rao, J. Solid State Chem. **114**, 297 (1995).

[13] H. L. Ju, J. Gopalakrishnan, J. L. Peng, Q. Li, G. C. Xiong, T. Venkatesan, and R. L. Greene, Phys. Rev. B **51**, 6143 (1995).

[14] A. Unishibara, Y. Moritomo, T. Arima, A. Asamitsu, G. Kido, and Y. Tokura, Phys. Rev. B **51**, 14 103 (1995).

[15] Y. Moritomo, A. Asamitsu, and Y. Tokura, Phys. Rev. B **51**, 16 491 (1995).

[16] C. Zener, Phys. Rev. **82**, 403 (1951).

[17] M. Verelst, N. Rangavittal, and C. N. R. Rao, J. Solid State Chem. **104**, 74 (1993); R. Mahesh, K. R. Kannan, and C. N. R. Rao, *ibid*. **114**, 294 (1995).

[18] J. A. M. Van Roosmalen, E. H. P. Cordfunke, R. B. Helmholdt, and H. W. Zandbergen, J. Solid State Chem. **110**, 100 (1994); J. A. M. Van Roosmalenand and E. H. P. Cordfunke, *ibid*. **110**, 109 (1994); M. Hervieu, R. Mahesh, N. Rangavittal, and C. N. R.

Rao, Eur. J. Solid State Inorg. Chem. **32**, 79 (1995).
[19] E. O. Wollan and W. C. Koehler, Phys. Rev. **100**, 545 (1995); J. B. Goodenough, *ibid*. **100**, 564 (1995).
[20] G. H. Jonker and J. H. Van Santen, Physica **16**, 337 (1950).
[21] N. F. Mott, *Metal Insulator Transitions* (Taylor and Francis, London, 1990).
[22] P. P. Edwards and M. J. Sienko, Phys. Rev. B **17**, 2575 (1978).
[23] J. P. Jan, Solid State Phys. **5**, 1 (1957).
[24] S. Banerjee and A. K. Raychaudhuri, Phys. Rev. B **52**, 3453 (1995); J. Phys. Condens. Matter **5**, L295 (1993).
[25] P. W. Anderson and H. Hasegawa, Phys. Rev. **100**, 675 (1955).
[26] V. G. Bhide, D. S. Rajoria, C. N. R. Rao, G. Rama Rao, and V. G. Jadhao, Phys. Rev. B **12**, 2832 (1975); P. Ganguly and C. N. R. Rao, in *Metallic and Non-Metallic States of Matter*, edited by P. P. Edwards and C. N. R. Rao (Taylor and Francis, London, 1985), p. 329.
[27] A. J. Mills, P. B. Littlewood, and B. I. Shraiman, Phys. Rev. Lett. **74**, 5144 (1995).
[28] A. Chainani, M. Mathew, and D. D. Sarma, Phys. Rev. B **47**, 15 (1993); **47**, 397 (1993).
[29] A. H. Morrish, *The Physical Principles of Magnetism* (Wiley, New York, 1965).
[30] R. Mahendiran, A. K. Raychaudhuri, A. Chainani, and D. D. Sarma, J. Phys. Condens. Matter **7**, L561 (1995).
[31] J. Tanaka and T. Mitsuhasi, J. Phys. Soc. Jpn. **53**, 1 (1984); **53**, 24 (1984).
[32] R. R. Heikes, in *Thermoelectricity*, edited by P. H. Egli (Wiley, New York, 1960); P. M. Chaikin and G. Bani, Phys. Rev. B **13**, 647 (1976).